Biophysical Journal Volume 99 September 2010 1783–1790

Water under the BAR

Edward Lyman, Haosheng Cui, and Gregory A. Voth*
Department of Chemistry, James Franck Institute, and Computation Institute, University of Chicago, Chicago, Illinois

ABSTRACT Many cellular processes require the generation of highly curved regions of cell membranes by interfacial membrane proteins. A number of such proteins are now known, and several mechanisms of curvature generation have been suggested, but so far a quantitative understanding of the importance of the various potential mechanisms remains elusive. Following previous theoretical work, we consider the electrostatic attraction that underlies the scaffold mechanism of membrane bending in the context of the N-BAR domain of amphiphysin. Analysis of atomistic molecular dynamics simulations reveals considerable water between the membrane and the positively charged concave face of the BAR, even when it is tightly bound to highly curved membranes. This results in significant screening of electrostatic interactions, suggesting that electrostatic attraction is not the main driving force behind curvature sensing, supporting recent experimental work. These results also emphasize the need for care when building coarse-grained models of protein-membrane interactions. These results are emphasized by simulations of oligomerized amphiphysin N-BARs at the atomistic and coarse-grained level. In the coarse-grained simulations, we find a strong dependence of the induced curvature on the dielectric screening.

INTRODUCTION

Biological membranes, both internally and at the plasma membrane, are observed to adopt a rich variety of topologies depending on the cellular processes involved (1,2). Some of these topologies, such as those observed at the necks of budding vesicles, involve regions of very high curvature (3). Considering that the energetic cost of rolling a flat membrane sheet into a membrane tubule of diameter 11 nm and length 5 nm is ~30 k_BT (assuming a bending modulus of 20 k_BT, where k_B is Boltzmann's constant and T is the absolute temperature) (4), it is clear that these structures are formed by the interaction of the lipid bilayer with curvature-generating proteins.

In vitro, at bulk concentrations of ~5 μM, the Bin/amphiphysin/Rvs domain-plus-N-terminal-amphipathic-helix (N-BAR domain) of amphiphysin remodels liposomes into tubules (5) with diameters similar to the necks of budding vesicles, where amphiphysin is found during clathrin-mediated endocytosis (3). The crystal structure of *Drosophila* amphiphysin revealed a coiled-coil homodimer, which presents to the membrane surface a number of conserved, positively charged residues on a concave face with a radius of 11 nm (5). Because the bilayers that amphiphysin targets are rich in negative charges, the amphiphysin structure led McMahon and Gallop (1) to suggest that electrostatic attraction between the concave face of the protein and the bilayer are responsible for curvature sensing and induction (i.e., the so-called scaffold mechanism). This hypothesis was supported by mutagenesis studies that demonstrate reduced tubulation efficiency upon mutation of the conserved positive charges (5) as well as rough calculations of the electrostatic binding energy based on results from model peptides (4).

However, other mutagenesis studies of amphiphysin point to the importance of the N-terminal helices for efficient remodeling (6). Indeed, tubulation has been observed by other domains lacking an obvious scaffold, but containing amphipathic moieties (7,8); tubulation of vesicles by only the H0 helix of amphiphysin has been observed experimentally (9), and theoretical study of the hydrophobic insertion mechanism has suggested that this mechanism alone is sufficient for tubulation (10). Insertion of amphipathic moieties into one leaflet can induce remodeling by generating a local spontaneous curvature (2,10); theoretical discussions of remodeling by N-BAR domains have therefore centered on the contributions of these two mechanisms (1,2,4,10–19). Indeed, recently it was found within a mean field approach that electrostatic contributions are sufficient to stabilize a local spontaneous curvature, demonstrating a way that the two mechanisms may work together (19). The amphipathic moieties are also known to be crucial to the ability of N-BAR domains to sense regions of high curvature (20) by identifying hydrophobic packing defects, as demonstrated recently by Bhatia et al. (21) and Hatzakis et al. (22) for the N-terminal amphipathic helix (henceforth called H0) of endophilin N-BAR. Bhatia et al. and Hatzakis et al. (21,22) have shown that the ability of H0 to sense membrane curvature is due not to an increased affinity of H0 for curved membranes, but rather to the increasing density of defects, and therefore binding sites, with increasing membrane curvature. Importantly for this work, they have demonstrated that sensing and induction of curvature are independent phenomena, and therefore observation of one does not imply the other.

The contribution of this work is to examine carefully the strength of the electrostatic attraction between the concave face of the N-BAR and the bilayer, to make progress toward disentangling the contributions of electrostatics

Submitted January 22, 2010, and accepted for publication June 28, 2010.
*Correspondence: gavoth@uchicago.edu
Editor: Nathan Andrew Baker.

0006-3495/10/09/1783/8 $2.00
doi: 10.1016/j.bpj.2010.06.074

and amphipathic insertions for generating membrane curvature and remodeling. Previous atomistic molecular dynamics (MD) simulations in our group have demonstrated local curvature generation by single N-BAR domains, via capture of spontaneous membrane undulations (13,15). Here, we show that even when the N-BAR domain is tightly bound to the membrane, considerable water remains between the protein and the membrane, resulting in significant electrostatic screening.

The result of this has important implications both for understanding membrane-remodeling mechanisms, as well as for the development of physically accurate coarse-grained models of the process. Coarse-grained models of the N-BAR/membrane system have been developed by us (11) and others (16,17,19,23) with the intention of bridging the gap between atomistic MD simulations, which access, at most, a few proteins, and experiments, which observe remodeling on micron-length scales. Experiments performed with F-BAR domains have demonstrated the importance of oligomerization of the protein coat in effecting remodeling, where lateral contacts between the proteins generate coats with beautiful helical symmetries (24). So far, the protein coat formed by N-BAR has yet to be resolved at sufficient resolution to determine the extent of oligomerization of the protein, and so the importance of ensemble effects in the case of N-BAR remodeling remains an open question. Indeed, N-BAR domains yield a diversity of remodeled structures, as recently shown in a combined mesoscopic simulation and experimental cryo-electron microscopy study (12). In this article, we argue that effective interactions in a coarse-grained context must be parameterized carefully to capture, with quantitative accuracy, the interactions between membrane and protein. In turn, this result has clear implications for the mechanism of membrane bending by N-BAR domain proteins.

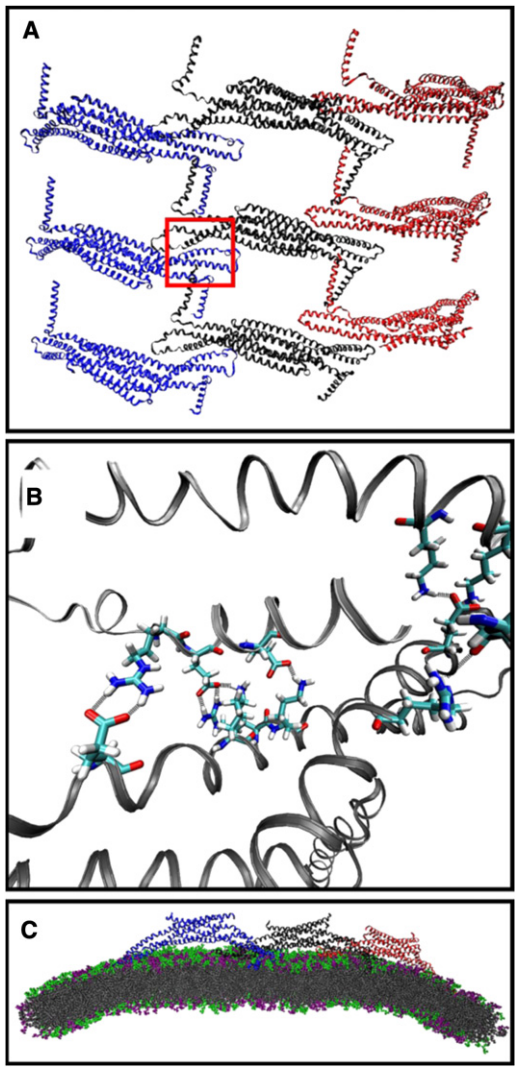

FIGURE 1 The configuration of the oligomer simulation. (*A*) Central simulation cell from the top and a periodic image on either side. (*B*) Close-up of the area highlighted by the red box in panel *A*, showing lateral contacts between neighboring rows of N-BARs. (*Dotted lines*) Favorable electrostatic interactions between atoms that are within 5 Å of each other. The view is from the membrane side and a piece of one helix of the scaffold is removed for clarity. (*C*) Final snapshot after 120 ns, which curved to a radius of 58 nm.

METHODS

Atomistic simulations

The computational protocol used for the NBR1 and NBR2 simulations was described previously (15). The initial structure for the oligomer simulation (Fig. 1, *A* and *B*) was constructed by assuming that the N-terminal helices dimerize and that favorable contacts are formed between the protein scaffolds, as discussed below. The N-terminal helix dimer was constructed by mapping out a two-dimensional potential energy surface assuming an antiparallel dimer. While this simple approach does not account for entropic contributions, it does predict a helix dimer in which favorable interactions are formed between charged residues on the lateral faces of the helices.

A set of three oligomerized N-BARs was then embedded in a patch of preequilibrated membrane consisting of 50:50 mixture of palmitoyl-oleoyl phosphatidylserine/phosphatidylcholine lipids. The membrane patch was sized so that the embedded N-BAR domains form a periodic array along the direction of the long axis of a membrane tubule, with the long axis of the protein wrapping around the tubule. In the other direction (along the long axis of the protein), the membrane patch was not periodic, but at the edges formed a half-cylindrical micelle instead, as shown later in Fig. 3 *C*. The lipid/protein system was solvated in a box of dimensions roughly 53 nm × 81 nm × 145 nm by 136,210 TIP3P water molecules, 1161 chloride ions, and 1761 sodium ions to create a neutral system with a salt concentration of 0.150 M. All calculations were performed using NAMD (25). The protein and lipids were modeled by the CHARMM22 (26) and CHARMM27 (27) empirical force field with the CMAP correction, with PS headgroups parameterized as described previously (15).

Electrostatic interactions were computed by the particle-mesh Ewald method, with a tolerance of 10^{-6} on the Ewald coefficient, a sixth-order interpolation between gird points, and a grid spacing of 1 Å. The system was minimized for 80,000 steps by a conjugate gradient search, then heated to 310 K with the protein and lipid restrained by harmonic restraints with a force constant of 100 kcal/mol Å^2, integrating the Langevin equation of motion with a time step of 2 fs, and constraining covalent bonds to hydrogens by the SHAKE algorithm (28). The system was then equilibrated for 5 ns (resampling velocities from a Boltzmann distribution at 310 K every

100 fs) with the harmonic restraints gradually reduced from 100 kcal/mol Å^2 to 1 kcal/mol Å^2. Once the restraints reached a value of 1 kcal/mol Å^2 they were turned off, and the system was evolved under conditions of constant pressure (1 atm) by coupling to a Langevin piston (29) with a period of 2 ps and constant temperature (310 K) controlled by a Langevin thermostat (30) with a damping frequency of 0.5 ps^{-1}.

Shape-based coarse-grained simulations

A shape-based coarse-grained model of amphiphysin N-BAR domain was developed and parameterized as described by Arkhipov et al. (16); some details are reproduced here for completeness. Each monomer of the protein dimer was mapped onto 25 coarse-grained sites, and the model was developed to enforce the symmetry of the dimer. Coarse-grained sites were connected by harmonic bonds if they were within 18 Å, and harmonic bonds and angles were parameterized by iterative refinement of the force constants to match the fluctuations as observed in atomistic simulation. Nonbonded interactions were modeled by Lennard-Jones and electrostatic interactions, with the CG sites inheriting the charge of the underlying atomistic sites. Each lipid was represented by two sites; a single such lipid represents a membrane area that corresponds to roughly 2.2 lipids. The composition of the bilayer was 70% DOPC, 30% DOPS. The lipids again inherit the charge of the underlying atomistic model. The DOPC lipids are therefore uncharged and the DOPS lipids carry a charge of $-2.2e$. The dimension of the membrane patch was 110 Å in the y direction and ~450 Å in the x direction, comprised of 662 coarse-grained lipids. Six copies of the CG N-BAR domain were placed in a latticelike arrangement with the long axis roughly parallel to x, as described in Yin et al. (23) and shown later in Fig. 5. The simulation box was 110 Å in the y direction, so that the system is an infinitely long lattice of protein in y. In x, the box was 1000 Å, leaving the ends of the membrane free to bend. In z, the box was 500 Å, leaving room for the membrane to bend without interacting with its periodic image. One-hundred-ninety-four ions with a $+2.2e$ charge were included for electroneutrality. Electrostatic interactions were calculated using a 35.0 Å cutoff, smoothed to zero at the cutoff with a switching function beginning at 20.0 Å. The Langevin equation of motion was integrated with the temperature of the bath set to 310 K, with damping frequency 2.0 ps^{-1}. The mass of the CG sites and the softness of the harmonic bonds permits much longer integration time steps compared to atomistic simulations; in this case, a 100-fs time step was used. Three values of the relative dielectric were studied: 1, 4, and 14. All input parameters and configurtion files are found in the Supporting Material.

RESULTS AND DISCUSSION

Oligomerized amphiphysin N-BAR

Electron microscopy of membrane tubules that are formed when vesicles are incubated with purified amphiphysin N-BAR suggests a coat of protein (5,31), though resolution sufficient to resolve the structure of the coat has yet to be achieved for any N-BAR domain. However, the coat of protein formed by an F-BAR domain has been resolved, revealing a striking pattern of helical symmetries (24). This has fueled speculation about the structure of N-BAR protein coats, though the data are, as yet, inconclusive. Here we present data for a putative oligomer structure (Fig. 1 *A*). Our structure is based on the identification of a region of charged residues that could form lateral contacts between side-by-side BAR domains, which are positioned to form a network of salt bridges (Fig. 1 *B*). We also assume that the N-terminal amphipathic helices dimerize, an assumption supported by experiments on the N-terminal helix alone (9). This oligomer structure—which appears to be distinct from any oligomer presented by Yin et al. (23)—yields an area density of protein of eight NBARs per 1000 nm^2.

A simulation of three oligomerized amphiphysin N-BAR domains was initiated by embedding the N-terminal helices in a flat membrane as described in Methods. After 120 ns, the curvature was calculated by fitting the membrane midplane to the arc of a circle. The curvature averaged over the entire membrane patch had equilibrated at ~0.017 nm^{-1} (a radius of 58 nm), which is significantly less than the experimentally observed curvature of amphiphysin-coated membrane tubules (0.04 nm^{-1}, or a radius of 25 nm) (5). The final simulation snapshot is shown later in Fig. 1 *C*. Curvature was measured by fitting the bilayer midplane, averaged over the final 20 ns of simulation, to the arc of a circle. This approach measures the global curvature, and ignores shorter wavelength membrane fluctuations. This is in contrast to the observation of very tight binding and high curvature in simulations of single amphiphysin N-BAR domains initiated from flat membranes (13,15). It is consistent with results presented by Yin et al. (23), who observed a maximal radius of curvature of 54 nm in atomistic simulations of (differently) oligomerized amphiphysin N-BARs after 300 ns. While it may be argued that our simulation may simply not be long enough, we observed that the system curvature was no longer changing, and therefore discontinued the computation. We therefore suggest instead that the initial configuration of several N-BAR domains on a flat membrane is perhaps not a wise choice. Indeed, it is not physical—in vitro, N-BAR domains are incubated with vesicles of a strictly controlled diameter, and binding and tubulation are very sensitive to the size of the vesicles (9). We suggest that the lack of convincing evidence of significant curvature generation in atomistic simulations of oligomerized N-BAR domains, despite the expenditure of enormous computational resources, suggests that such atomistic simulations may not be the conclusive vehicle for studying membrane-remodeling phenomena on lengthscales beyond single proteins (11,12,14). After all, in vitro tubulation assays with N-BAR domains are not performed on thin strips of membranes with free ends, but on (carefully size-selected) vesicles.

Dielectric screening of BAR-membrane interactions in atomistic simulation

We first present new analysis of two independent simulation trajectories, each of a single amphiphysin N-BAR domain bound to a membrane, both of which were presented in an earlier article (15). The two trajectories differ in the orientation of the concave face of the BAR relative to the membrane. In trajectory NBR1, the BAR is oriented for maximum contact between the concave face and the

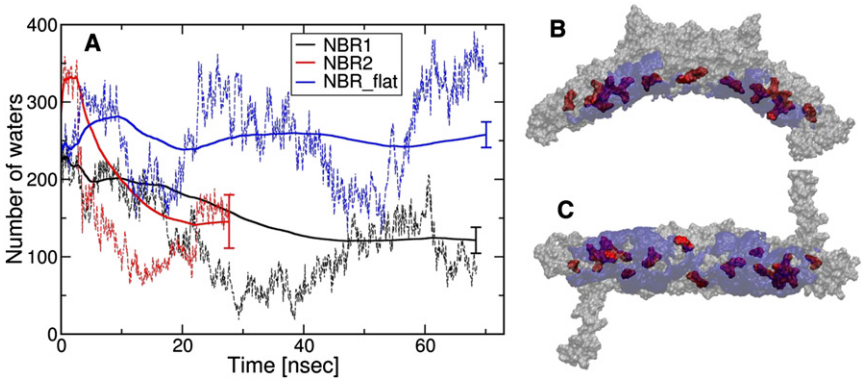

FIGURE 2 (*A*) Number of water molecules in between the concave face of the BAR and membrane for three independent simulations of amphiphysin N-BAR domains bound to the membrane by embedded N-terminal helices (*dashed lines*). The running averages (*solid lines*) with the standard error computed by dividing the trajectory into 10 equal length blocks (indicated by *error bar*). (*B*, *side view* and *C*, *bottom view*) Occupancy of water molecules under the arch of the BAR, averaged over the NBR1 trajectory from 30 ns onward (tight binding). The 30% occupancy isosurface (*translucent blue shading*) shows regions where water molecules are found at least 30% of the time. Surface of the N-BAR (*light shading*); conserved positive residues are under the arch (*red*). All molecular renderings were made with VMD (35).

membrane, resulting in the tightest interaction between the conserved positive charges on the concave face and the membrane. (We present here an extended version of this trajectory.) In trajectory NBR2, the BAR is observed to tilt a bit away from the membrane, resulting in a different binding mode and less local curvature. We also present a new trajectory (called NBR_flat) in which a single N-BAR is bound to a membrane by the N-terminal helices, but no curvature induction is observed. Also included in the analysis are the three N-BAR domains from the oligomer simulation, described in the previous section.

Fig. 2 demonstrates that, even when the membrane is maximally curved and the BAR is tightly bound (trajectory NBR1), considerable water remains between the positively charged concave arch of the protein and the membrane. The count in Fig. 2 *A* is defined by slicing the system along the long axis of the BAR domain, and then for each slice defining the space that is between as bounded by the ester groups of the lipids (because these groups define the edge of the interfacial membrane region) and the α-carbons of the protein backbone nearest the membrane. After 30 ns, the protein in simulation NBR1 is tightly bound and the membrane highly curved, and the number of waters is observed to fluctuate between 20 and 200. A slow oscillation in the amount of water in between the membrane and the protein is observable, owing to the undulation of the membrane under the protein. The slow fluctuation means that the mean (*solid line*) is best understood as an estimate up to the precision indicated by the error bar, which represents an estimate of the standard error based on the variance among 10 nonoverlapping segments of the trajectory. An oscillation with a similar period is also observable in the trajectory which fails to measurably bend (NBR_flat), though as one might expect, there is considerably more interstitial water. Finally, we turn our attention to the three copies of the protein in the oligomer simulation (Fig. 3). There is considerable variation in how closely the three copies associate with the membrane, spanning the range observed in Fig. 2 from tightly bound membranes to flat membranes.

Fig. 2 *B* depicts how much water is in the neighborhood of positive charges on the arch of the BAR, averaged over the tightly bound portion of trajectory NBR1, from 30 ns onward. It is clear that several positive residues are at least partially solvated, even during the tightest binding. While this water is clearly not behaving as in the bulk phase, it is interesting to ask whether it might contribute some dielectric screening of the charged interactions between protein and membrane. This is discussed in the next section.

How effective is the residual water in screening the interactions between positively charged residues of the BAR and the negatively charged PS headgroups? Hess et al. (32) have shown that the dielectric screening of an ion pair by the fluctuating dipole of the intervening water is approximated surprisingly well by the Boltzmann-inverted ion pair distribution function. The same analysis for our system is presented in Fig. 4, where the potential of mean force (PMF) as a function of distance r between the conserved positive

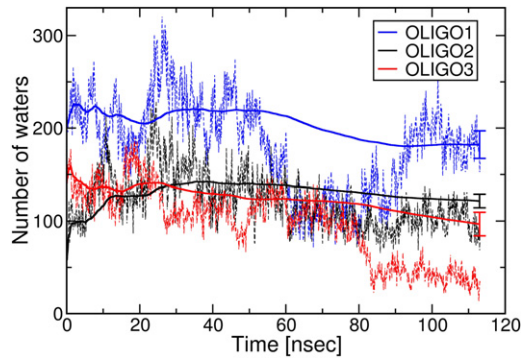

FIGURE 3 The number of water molecules in between the concave face of the BAR and membrane for the three proteins in the oligomer simulation. The color of the time traces matches the color of the proteins in Fig. 1; the meaning of the dashed and solid lines and the error bars are explained in Fig. 2's legend.

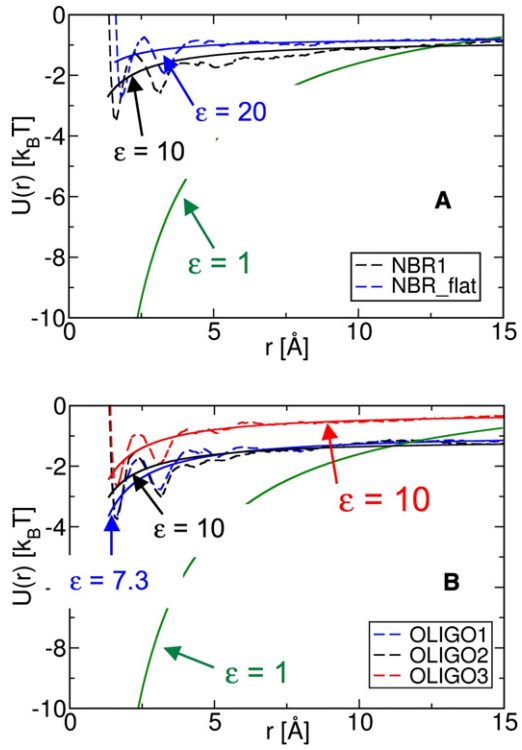

FIGURE 4 (*A* and *B*) The effective dielectric constant for all six datasets is computed by fitting a potential of the form $q_1q_2/\varepsilon\varepsilon_0 r$ (*red line*) to the long-range part of the approximate potential of mean force (PMF) between negatively charged oxygens (with charge q_1) of the phosphatidylserine headgroups and positively charged hydrogens (with charge q_2) of Lys and Arg side chains under the concave face of the BAR. Panel (*A*) corresponds to the single N-BAR data in Fig. 2. Panel (*B*) corresponds to the oligomer data in Fig. 3.The free parameter is the dielectric constant, ε; ε_0 is the permittivity of the vacuum. The PMF is computed by Boltzmann inversion of the radial distribution function, averaged over the conserved positive charges under the arch of the protein. The fit is performed over the entire range of the potential, following Hess et al. (32). For comparison, the shape of the bare Coulomb ($\varepsilon = 1$) potential is shown (*green*).

residues of the arch and the PS headgroups is fitted to a $1/r$ potential. The PMF, denoted $U(r)$, is computed by Boltzmann inversion (33) of the radial distribution function,

$$g(r) : U(r) = -k_B T \ln(g(r)),$$

where k_B is Boltzmann's constant and T is temperature. Because the electrostatic potential $U_{el}(r)$ between a pair of point charges screened by a polarizable medium is given by

$$U_{el}(r) = q_1 q_2 / \varepsilon_0 \varepsilon_r r,$$

the only free parameter of the fit is ε_r, the relative dielectric permittivity. For the six bound N-BAR domains analyzed here, the dielectric constant (ε) that scales the bare Coulomb interaction ranges from 10 to 20, always intermediate between the vacuum ($\varepsilon = 1$) and pure bulk water ($\varepsilon = 80$ at 293 K). It is noteworthy that the dielectric constants track roughly with the amount of water observed, on average, between the protein and the membrane, with more water corresponding to a higher dielectric. (Note that the effective dielectric between protein and membrane estimated in this manner also includes dipole fluctuations of other side chains and lipid headgroups. As these groups are far less mobile than the water, they contribute much less to the screening than the residual water.) For reference, the vacuum Coulomb interaction is also shown, i.e., a dielectric constant of 1, which has been used in some coarse-grained models of N-BAR tubulation (16,17,23), and which yields an electrostatic interaction that is between 10 and 20 times too strong. While the electrostatic potential due to the membrane experienced by a protein in bulk salt solution is of course renormalized by the mobile ions, in this case we are concerned with the protein-membrane interaction once the N-terminal helices are embedded. In this case, no salt was observed in the interstitial space between the protein and the membrane.

We also calculated the fraction of time (averaged only over the period of the trajectory during which curvature has equilibrated) that key positively charged residues are in contact with negatively charged lipids, as shown in Table 1. (Here we focus only on contacts between PS headgroups and the BAR, because BAR domains do not remodel purely zwitterionic membranes.) Even for the most tightly bound and highly curved membrane (NBR1), we observe that of the 24 possible contacts, only three are maintained >90% of the time, and two more contacts are formed ~50% of the time. Even fewer contacts are formed for the NBR2 trajectory. These results make sense in light of the analysis of water screening just presented, but are at odds with the idea that an unscreened Coulomb interaction accurately represents the interaction between the N-BAR and the membrane, as has been hardwired into some recently published coarse-grained models (16,17,23).

TABLE 1 Fraction of time that key positively charged residues on the arch of the N-BAR are in contact with negatively charged phosphatidylserine (PS) headgroups of the lipids

	NBR1		NBR2	
	Chain A	Chain B	Chain A	Chain B
R55*†	0.00	0.01	0.00	0.00
K58*†	0.98	0.39	0.09	0.01
R65†	0.02	0.93	0.00	0.00
R68*	0.00	0.00	0.00	0.00
K75	0.00	0.00	0.00	0.10
K132*	0.04	0.11	0.14	0.00
K133	0.93	0.50	0.15	0.69
K134*	0.00	0.00	0.00	0.00
K137*	0.00	0.07	0.01	0.80
K138*	0.00	0.00	0.64	0.00
R140*	1.00	0.00	0.00	0.96
R149*	0.00	0.00	0.00	0.00

A contact is defined as a distance of <5 Å between the oxygen of the PS headgroup and the hydrogen of the positive residue.
*Conserved residues.
†Residues located under the highest part of the arch.

Based on the results in Fig. 4 and Table 1, we can offer an estimate for the electrostatic contribution to the free energy that is acquired when a flat membrane—with an N-BAR domain already bound by its N-terminal helices—is locally curved to bring a positively charged residue into close apposition with a PS headgroup. If we take the curve for NBR1, and compare the value of the fit at $r = 15$ Å to the value at the first minimum of the PMF, we get roughly 1 k_BT per H-O pair. Table 1 tells us that there are three H-O pairs in simulation NBR1 that sit at the first minimum of the PMF; we estimate that these three pairs together contribute 3 k_BT to the binding of a curved versus a flat membrane. This modest free energy gain is probably sufficient to stabilize locally curved membranes, when working in concert with a local spontaneous curvature created by insertion of the N-terminal helices, as suggested recently by Khelashvili et al. (19) and seen previously in the all-atom MD simulations of Blood and co-workers (13,15). We next investigate the importance of the dielectric screening between protein and membrane in developing coarse-grained models of membrane remodeling.

Dielectric-dependent remodeling in coarse-grained simulations

Clearly, coarse-grained models are needed to address the problem of membrane remodeling beyond the lengthscale of a few proteins. It is important, however, that such models are predictive, in the sense that observables on the coarse-grained lengthscale—curvature, for example—are either 1), not dependent on tunable parameters, or 2), those parameters are motivated in some clearly justifiable way, by experiment or by a simulation at shorter length- and timescales.

Here, we have argued based on atomistic simulation data that in the problem of membrane remodeling by N-BAR domains, electrostatic interactions between the protein and membrane are screened by interstitial water, resulting in a relative dielectric of between 10 and 20. Many general-purpose coarse-grained models (MARTINI, for example (34)) incorporate a relative dielectric to attenuate electrostatic interactions. Our own coarse-grained model of membrane remodeling by amphiphysin on liposome scales (11) incorporated membrane-protein interactions that were strongly attenuated, accounting for Debye screening by mobile salt ions, as did recent work at the continuum level by Khelashvili et al. (19). Other recent work, on the other hand, has modeled electrostatic interactions at the coarse-grained level by a bare Coulomb interaction (16,17,23). We therefore address here a very specific question: Does the curvature induced by a coarse-grained N-BAR-membrane model depend on the value of the relative dielectric?

The top two panels of Fig. 5 show two views of the starting configuration of a coarse-grained model of six amphiphysin N-BAR domains, in a previously published putative oligomer configuration. The model was developed

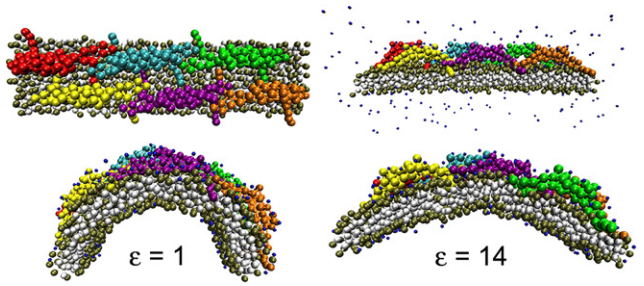

FIGURE 5 (*Upper-left panel*) Top view of the starting configuration of the six-amphiphysin N-BAR SBCG simulation (counterions omitted for clarity). (*Upper-right panel*) Side view of the starting configuration of the SBCG simulations, showing counterions. (*Lower-left panel*) Final configuration of the SBCG simulation with the relative dielectric set to 1. (*Lower-right panel*) Final configuration of the SBCG simulation with the relative dielectric set to 14.

using the shape-based coarse-graining method software (16,17,23) and distributed with VMD version 1.8.7 (35). Simulations were performed at three different values of ε: $\varepsilon = 1$, 4, and 14. The final configurations of the $\varepsilon = 1$ and $\varepsilon = 14$ simulations, after 40 M time steps, are shown in the bottom panel. Clearly, the attenuation of the electrostatic interaction has a dramatic effect on the curvature. The influence of the relative dielectric is quantified in Fig. 6. For all three values of ε, the position of the membrane midplane was averaged over the final 1000 configurations (10^7 time steps) of the simulation. The midplane was then fit to the arc of a circle to quantify the radius of curvature. Employing a value for ε that is consistent with that obtained from our atomistic observations reduces the induced radius of curvature by more than a factor of two.

SUMMARY AND CONCLUSIONS

We have presented atomistic MD simulation data demonstrating that there is significant screening of electrostatic interactions between charged lipids and charged residues

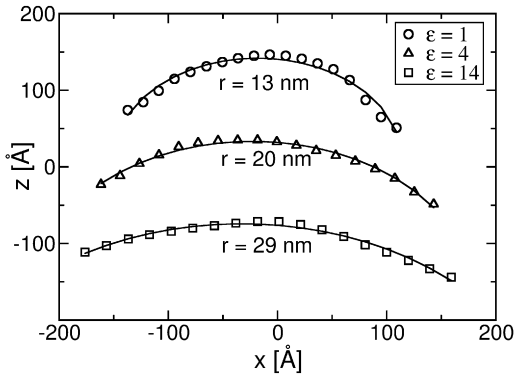

FIGURE 6 Position of the membrane midplane (*symbols*) averaged over the last 1000 configurations of each of the three SBCG simulations. Also shown (*solid lines*) are the fits of each to the arc of a circle, with the radius of the fit written below each data set.

on the concave face of N-BAR domains, even when the protein is as tightly bound as is physically reasonable.

Our first point is that, based on Boltzmann inversion of pairwise radial distribution functions (32), we estimate that electrostatic interactions between the concave face of the BAR and the membrane contribute ~3 k_BT to the membrane-protein interaction. This is lower than a previous theoretical estimate (7 k_BT) of the electrostatic interaction needed for a BAR domain to form a membrane tubule (4), but is probably sufficient for a mechanism that combines amphipathic helix insertion and electrostatic attraction (1,2,18,19). As a second point, we have also discussed simulations of oligomerized N-BAR domains which failed to appreciably bend initially flat membranes, in agreement with previously published atomistic simulations of oligomerized N-BAR domains (23). This second point speaks to the importance of accurate coarse-grained models for the study of membrane remodeling processes at larger length- and timescales. The first point, however, speaks to the importance of considering carefully how those models are developed, in order that the correct physics is captured in effective interactions at the coarse-grained scale.

The parameters that govern, for example, the strength of interactions between proteins and membranes in a coarse-grained context, are not simply adjustable parameters. Instead, effort must be made to connect coarse-grained, effective interactions to the relevant physics at shorter length- and timescales. This approach may yield genuinely predictive models, rather than phenomenological models tuned to reproduce the same long length- and timescale phenomena that they purport to explain. The importance of careful coarse-grained model parameterization was demonstrated with simulations of membrane deformation using the shape-based coarse-graining methodology (16,17,23), where we have found that the modeling of effective electrostatic interactions has a dramatic effect on the observed curvature.

SUPPORTING MATERIAL

Input configurations, parameters, and simulation configuration files for the SBCG simulations are available at http://www.biophysj.org/biophysj/supplemental/S0006-3495(10)00845-3.

Calculations were performed on machines housed at the Pittsburgh Supercomputing Center (Big Ben), the Texas Advanced Computing Center (Ranger), and the National Institute for Computing Sciences (Kraken). The authors thank Phil Blood and Richard Swenson for assistance with the simulations, Gary Ayton for suggesting the analysis in Fig. 2, and Vinzenz Unger and Carsten Mim for many thoughtful discussions. The early stages of this research were carried out in the Center for Biophysical Modeling and Simulation, University of Utah.

This work was supported by the National Institutes of Health (grant No. R01-GM063796). The calculations were enabled by a grant through the TeraGrid program of the National Science Foundation.

REFERENCES

1. McMahon, H. T., and J. L. Gallop. 2005. Membrane curvature and mechanisms of dynamic cell membrane remodeling. *Nature.* 438:590–596.
2. Zimmerberg, J., and M. M. Kozlov. 2006. How proteins produce cellular membrane curvature. *Nat. Rev. Mol. Cell Biol.* 7:9–19.
3. Slepnev, V. I., and P. De Camilli. 2000. Accessory factors in clathrin-dependent synaptic vesicle endocytosis. *Nat. Rev. Neurosci.* 1: 161–172.
4. Zimmerberg, J., and S. McLaughlin. 2004. Membrane curvature: how BAR domains bend bilayers. *Curr. Biol.* 14:R250–R252.
5. Peter, B. J., H. M. Kent, …, H. T. McMahon. 2004. BAR domains as sensors of membrane curvature: the amphiphysin BAR structure. *Science.* 303:495–499.
6. Farsad, K., N. Ringstad, …, P. De Camilli. 2001. Generation of high curvature membranes mediated by direct endophilin bilayer interactions. *J. Cell Biol.* 155:193–200.
7. Martens, S., M. M. Kozlov, and H. T. McMahon. 2007. How synaptotagmin promotes membrane fusion. *Science.* 316:1205–1208.
8. Ford, M. G. J., I. G. Mills, …, H. T. McMahon. 2002. Curvature of clathrin-coated pits driven by epsin. *Nature.* 419:361–366.
9. Fernandes, F., L. M. S. Loura, …, M. Prieto. 2008. Role of helix 0 of the N-BAR domain in membrane curvature generation. *Biophys. J.* 94:3065–3073.
10. Campelo, F., H. T. McMahon, and M. M. Kozlov. 2008. The hydrophobic insertion mechanism of membrane curvature generation by proteins. *Biophys. J.* 95:2325–2339.
11. Ayton, G. S., E. Lyman, and G. A. Voth. 2010. Hierarchical coarse-graining strategy for protein-membrane systems to access mesoscopic scales. *Faraday Discuss.* 144:347–357, discussion 445–481.
12. Ayton, G. S., E. Lyman, …, G. A. Voth. 2009. New insights into BAR domain-induced membrane remodeling. *Biophys. J.* 97:1616–1625.
13. Blood, P. D., R. D. Swenson, and G. A. Voth. 2008. Factors influencing local membrane curvature induction by N-BAR domains as revealed by molecular dynamics simulations. *Biophys. J.* 95:1866–1876.
14. Ayton, G. S., P. D. Blood, and G. A. Voth. 2007. Membrane remodeling from N-BAR domain interactions: insights from multi-scale simulation. *Biophys. J.* 92:3595–3602.
15. Blood, P. D., and G. A. Voth. 2006. Direct observation of Bin/amphiphysin/Rvs (BAR) domain-induced membrane curvature by means of molecular dynamics simulations. *Proc. Natl. Acad. Sci. USA.* 103:15068–15072.
16. Arkhipov, A., Y. Yin, and K. Schulten. 2008. Four-scale description of membrane sculpting by BAR domains. *Biophys. J.* 95:2806–2821.
17. Arkhipov, A., Y. Yin, and K. Schulten. 2009. Membrane-bending mechanism of amphiphysin N-BAR domains. *Biophys. J.* 97:2727–2735.
18. Gallop, J. L., and H. T. McMahon. 2005. BAR domains and membrane curvature: bringing your curves to the BAR. *Biochem. Soc. Symp.* 72:223–231.
19. Khelashvili, G., D. Harries, and H. Weinstein. 2009. Modeling membrane deformations and lipid demixing upon protein-membrane interaction: the BAR dimer adsorption. *Biophys. J.* 97:1626–1635.
20. Drin, G., J.-F. Casella, …, B. Antonny. 2007. A general amphipathic α-helical motif for sensing membrane curvature. *Nat. Struct. Mol. Biol.* 14:138–146.
21. Bhatia, V. K., K. L. Madsen, …, D. Stamou. 2009. Amphipathic motifs in BAR domains are essential for membrane curvature sensing. *EMBO J.* 28:3303–3314.
22. Hatzakis, N. S., V. K. Bhatia, …, D. Stamou. 2009. How curved membranes recruit amphipathic helices and protein anchoring motifs. *Nat. Chem. Biol.* 5:835–841.

23. Yin, Y., A. Arkhipov, and K. Schulten. 2009. Simulations of membrane tubulation by lattices of amphiphysin N-BAR domains. *Structure.* 17:882–892.

24. Frost, A., R. Perera, …, V. M. Unger. 2008. Structural basis of membrane invagination by F-BAR domains. *Cell.* 132:807–817.

25. Phillips, J. C., R. Braun, …, K. Schulten. 2005. Scalable molecular dynamics with NAMD. *J. Comput. Chem.* 26:1781–1802.

26. MacKerell, A. D., D. Bashford, …, D. Karplus. 1998. All-atom empirical potential for molecular modeling and dynamics studies of proteins. *J. Phys. Chem. B.* 102:3586–3616.

27. Feller, S. E., and A. D. MacKerell. 2000. An improved empirical potential energy function for molecular simulations of phospholipids. *J. Phys. Chem. B.* 104:7510–7515.

28. Ryckaert, J.-P., G. Ciccotti, and H. J. C. Berendsen. 1977. Numerical integration of the Cartesian equations of motion of a system with constraints: molecular dynamics of *n*-alkanes. *J. Comput. Phys.* 23:327–341.

29. Feller, S. E., Y. Zhang, …, B. R. Brooks. 1995. Constant pressure molecular dynamics simulation: the Langevin piston method. *J. Chem. Phys.* 103:4613–4621.

30. Grest, G. S., and K. Kremer. 1986. Molecular dynamics simulation for polymers in the presence of a heat bath. *Phys. Rev. A.* 33:3628–3631.

31. Masuda, M., S. Takeda, …, N. Mochizuki. 2006. Endophilin BAR domain drives membrane curvature by two newly identified structure-based mechanisms. *EMBO J.* 25:2889–2897.

32. Hess, B., C. Holm, and N. van der Vegt. 2006. Osmotic coefficients of atomistic NaCl (aq) force fields. *J. Chem. Phys.* 124:164509.

33. Reith, D., M. Pütz, and F. Müller-Plathe. 2003. Deriving effective mesoscale potentials from atomistic simulations. *J. Comput. Chem.* 24:1624–1636.

34. Marrink, S. J., H. J. Risselada, …, A. H. de Vries. 2007. The MARTINI force field: coarse-grained model for biomolecular simulations. *J. Phys. Chem. B.* 111:7812–7824.

35. Humphrey, W., A. Dalke, and K. Schulten. 1996. VMD: visual molecular dynamics. *J. Mol. Graph.* 14:33–38, 27–28.

36. Reference deleted in proof.